Physicochem. Probl. Miner. Process., 61(6), 2025, 214348

http://www.journalssystem.com/ppmp

Physicochemical Problems of Mineral Processing

ISSN 1643-1049

Separation of calcium, magnesium, and phosphorus from roasted phosphate tailings via a two-step ammonium-salt leaching process

Dandan Liu [1,2], Xiong Tong [1,2], Peiqiang Fan [1,2,3], Chang Shen [1,2], Yongjie Guo [3], Lingpan Du [3]

[1] Faculty of Land Resource Engineering, Kunming University of Science and Technology, Kunming 650000, China

[2] National Local Joint Engineering Research Center for Green Utilization of Metal Tailings Resources, Kunming 650093, China

[3] National Engineering and Technology Research Center for Development & Utilization of Phosphate Resources, Kunming 652500, China

Corresponding author: kgxiongtong@163.com (Xiong Tong)

Abstract: Phosphate tailings, rich in calcium, magnesium, and phosphorus, are conventionally processed through roasting and leaching. We propose two-stage ammonium-salt leaching as a new separation method for calcined phosphate tailings. In the first stage, calcium extraction reached 84.67% through Box-Behnken-optimized ammonium chloride leaching (20 °C, NH_4Cl/tailings mass ratio of 0.98, liquid-solid ratio of 9.78, pH 8.5, 40 min), following internal diffusion-controlled kinetics (E_a = 2.24 kJ/mol), as described by: $2(1-x)-3(1-x)^{2/3}=3.7234\times10^{-2}\cdot\exp(-2.2436\times10^{-2}/RT)t$. The second stage achieved 95.21% magnesium leaching via Box–Behnken-optimized ammonium sulfate conditions (85.14 °C, $(NH_4)_2SO_4$/residue ratio of 1.2, liquid-solid ratio of 12.1, pH 7, 60 min), exhibiting chemical-reaction-controlled kinetics (E_a = 37.58 kJ/mol), described by: $1-(1-x)^{1/3}=3.4099\times10^{3}\exp(-3.7584\times10^{4}/RT)t$. The near-neutral leaching system facilitates reagent regeneration via ammonia recovery, mitigating equipment corrosion and diminishing chemical consumption, whilst co-producing high-value-added products—namely, Type 96 calcium hydroxide (HG/T 4120-2024) and Type II-B magnesium hydroxide (HG/T 3607-2024). The residual slag can be directly utilized as flotation feed for phosphorus recovery, ensuring complete tailings valorization without secondary waste generation.

Keywords: phosphate tailings, ammonia cycle, surface response, leaching kinetics, precipitate

1. Introduction

Phosphorus is an indispensable core resource in modern agriculture. However, its extraction is challenging because of the low quality of phosphate rock and the large amount of tailings produced during the beneficiation process. Thus, the recycling and utilization of phosphate tailings have become a major bottleneck limiting sustainable development. Phosphate tailings mainly originate from the flotation process of phosphorus ore (e.g., positive flotation, reverse flotation) and the low-grade phosphorus slag (in which the P_2O_5 content is usually <10%) that remains after the separation of impurities by physical or chemical methods(Yu et al., 2024). According to 2025 USGS statistics, global phosphate rock production will continue to grow, in terms of P_2O_5 content, and is expected to reach an average annual growth rate of 1.7% between 2024 and 2028, with production exceeding 70.6 million tons in 2028(Mineral commodity summaries 2025, 2025). China is the world's largest phosphate ore and rock producer and holds the world's second-largest phosphate rock reserve. In 2024, China produced approximately 11,000 million tons of phosphate rock. Although this was an increase of 4.76% year-on-year, it was still limited by the level of beneficiation technology, with approximately 30%–40% of the phosphorus ore going into the tailings and annual emissions of more than 10 million tons(Gu et al., 2025; Mineral commodity summaries 2025, 2025; Chen et al., 2024). Currently, the comprehensive utilization efficiency of phosphate tailings is only approximately 10%. Accumulation of these tailings results in the wastage of resources (such as phosphorus, calcium, and magnesium) and poses an

DOI: 10.37190/ppmp/214348

ecological risk owing to the migration of heavy metals and the release of radioactive substances(Y. Xiao et al., 2024). With the depletion of high-grade phosphate resources, improving the resource utilization of phosphate tailings has become a priority for realizing clean and sustainable production of phosphorus(Amar et al., 2022).

Phosphate tailings consist mainly of dolomite, fluorapatite, and quartz, and are rich in calcium, magnesium, and phosphorus. Most of the phosphate tailings are usually used as filling materials, whereby they are compounded with cementitious materials and used to fill the void areas of mines. There is also direct utilization in agriculture, environmental protection, and construction. For example, phosphate tailings can be used as a soil conditioner after activation treatment to produce heavy-metal adsorbent materials, ultralight ceramic granules, sintered bricks, and cement admixtures(Fu et al., 2024; T. Xiao et al., 2024; Jiang et al., 2023). Although these applications effectively consume the phosphate tailings, a part of the valuable elements (Ca, Mg, P) cannot be recovered in considerable quantities. The current technology for extracting valuable components from phosphate tailings mainly focuses on high-temperature calcination and acid leaching. Although high-temperature calcium and magnesium separation yields light calcium carbonate and other high-value products, the high energy cost significantly restricts its industrial application(Z. Ma et al., 2025). Although wet acid leaching can realize efficient extraction of phosphorus, it requires high acid consumption and produces acidic wastewater containing fluorine and heavy metals, while underutilizing other elements(Ding et al., 2025; Ye et al., 2024; Yu et al., 2023). Specifically, it is difficult to realize selective extraction of phosphorus from fluorapatite ($Ca_5(PO_4)_3F$) using conventional hydrometallurgy because of its dense crystal structure and strong fluoride-encapsulation effect.

In this study, we propose a two-step ammonium-salt leaching process for the selective separation of calcium, magnesium, and phosphorus. The ammonium salts enable the selective leaching of calcium and magnesium components. In the first stage, calcium components are preferentially leached in a weakly alkaline solution (pH 8.5), forming soluble calcium salts. In the second stage, the pH is adjusted to neutral (pH 7.0) to selectively leach magnesium components. The ammonia gas generated from the two leaching processes is collected and used to synthesize the leaching medium in the primary leaching process, ultimately yielding a silicon-containing, high-grade phosphorus-rich slag (P_2O_5 content > 17%) suitable for subsequent phosphorus recovery. Following two rounds of precipitation, separation, and drying, calcium hydroxide and magnesium hydroxide products meeting industrial standards are obtained, respectively.

2. Materials and methods

2.1. Mineral samples and reagents

Phosphate tailings used in this study were collected from the phosphate industry in Yunnan Province after the flotation of phosphorus ore. Phosphate tailings were dynamically roasted at 900 °C for 20 min for subsequent leaching. Analytical-grade ammonium chloride, ammonium sulfate, ammonium acetate, ammonium bicarbonate, hydrochloric acid, sulfuric acid, and sodium hydroxide were obtained from Sinopharm Chemical Reagent Co. All solutions were prepared using deionized water.

2.2. Two-stage leaching test

Fig. 1 shows the process flow diagram for separating calcium, magnesium, and phosphorus from calcined phosphate tailings using a two-stage ammonia leaching method (with ammonia recycling) to obtain economically valuable calcium-magnesium products. In the first stage, hydrochloric acid is injected into the reaction system, and ammonium chloride is synthesized into the leaching medium by circulating ammonia; the chemical reaction is shown in Eq. (1). Ammonium chloride then reacts selectively with the calcium oxide in the raw material, generating soluble calcium chloride and releasing ammonia, as shown in Eq. (2). After vacuum filtration, the first-stage leaching residue is used in the second leaching stage. Magnesium oxide is leached with ammonium sulfate solution under heating conditions to produce soluble magnesium sulfate and release ammonia gas, as shown in Eq. (3). After reaching the set leaching time, vacuum filtration yields the filtrate and segmented filter residue. The ammonia generated in the two-stage leaching process is recovered by condensation and re-entered into

the first-stage leaching reactor to participate in the synthesis of ammonium chloride. This results in a self-supporting reaction system, which relies on ammonia recycling to reduce the consumption of reagents. Add sodium hydroxide to Leachate I and Leachate II to adjust the pH, then filter and dry to obtain calcium hydroxide and magnesium hydroxide products, respectively. The ionic equations are shown in Eqs. (4) and (5). This process employs ammonium chloride and ammonium sulfate as the primary leaching agents for calcium and magnesium, respectively. Through the hydrolysis equilibrium of NH_4^+, a naturally mild, near-neutral buffered environment is established within the system. This enables highly selective, stepwise leaching of calcium and magnesium while ensuring valuable coexisting elements like phosphorus remain stably retained in the leaching residue. Simultaneously, the continuously volatilizing NH_3 generated during the reaction not only drives the equilibrium to the right but also prevents excessive H^+ accumulation that could acidify the system. This synergistic mechanism guarantees selective leaching of calcium and magnesium while stabilizing phosphorus retention within the residue. Compared to traditional acid leaching, ammonium salt leaching significantly reduces equipment corrosion risks and simplifies wastewater treatment challenges.

$$NH_3(g) + HCl\ (l) \rightarrow NH_4Cl(l) \quad (1)$$

$$2NH_4Cl + CaO \rightarrow CaCl + 2NH_3(g) + H_2O \quad (2)$$

$$(NH_4)_2SO_4 + MgO \xrightarrow{\Delta} MgSO_4 + 2NH_3(g) + H_2O \quad (3)$$

$$Ca^{2+}(aq) + 2OH^- \rightarrow Ca(OH)_2(s) \quad (4)$$

$$Mg^{2+}(aq) + 2OH^- \rightarrow Mg(OH)_2(s) \quad (5)$$

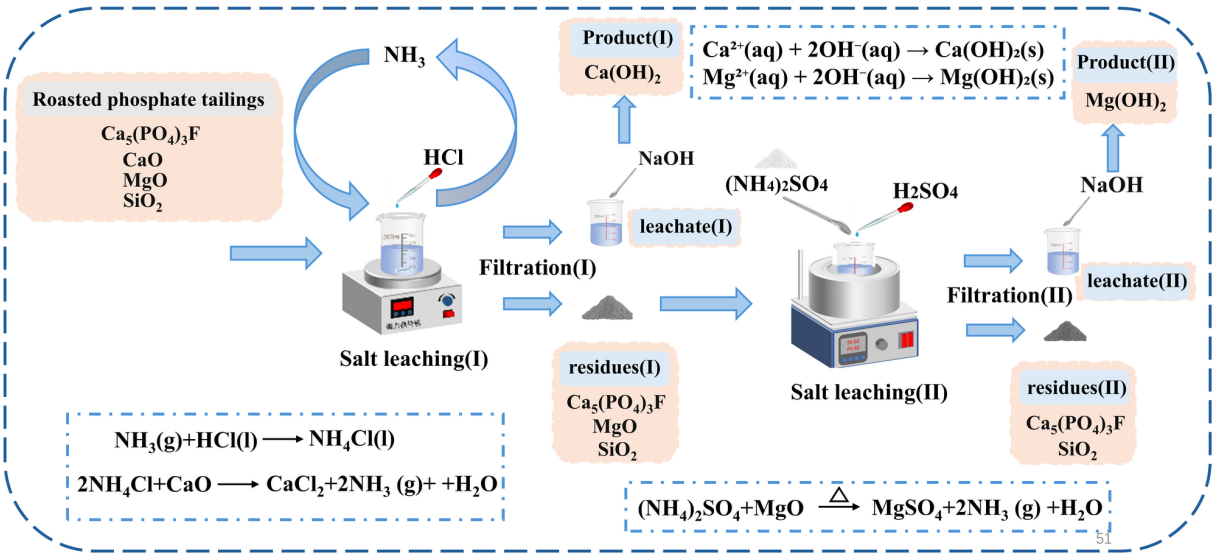

Fig. 1. Lowchart of the two-stage leaching-precipitation process

2.3. Analysis methods

The ore sample (10.00 g), weighed accurately using an electronic balance, was transferred into an 80 mL glass beaker. A specific volume of leaching agent was added, and the mixture was stirred magnetically. Upon completion of the leaching process, the mixture was filtered, and the volume of the filtrate was recorded. The solid residue was then transferred to a new 80 mL beaker, mixed with another specific volume of leaching agent, and heated in a water bath at a preset temperature for secondary leaching. After the set time, the mixture was filtered again. The volume of the second filtrate was measured, and the solid residue was dried and stored. The rates of calcium and magnesium leaching (ε_M) were calculated according to Eq. (6):

$$\varepsilon_M = \frac{c_M v_M}{m_M \alpha_M} \times 10000 \quad (6)$$

Among which, ε_M represents the element M leaching rate, %; c_M represents the concentration of element M in the leaching solution, g/L; v_M represents the volume of leached liquid, L; m_M represented the mass of the sample used in the test, g; α_M represented the element M grade in sample, %.

The concentrations of major elements (P, Ca, Mg, Si, Fe, F, Al) in both the calcined tailings and the leachates were determined by inductively coupled plasma optical emission spectroscopy (ICP-OES). The mineralogical characteristics of the solid samples were analyzed through chemical analysis, laser particle size analysis, scanning electron microscopy with energy-dispersive X-ray spectroscopy (SEM-EDS), and X-ray diffraction (XRD). The quality of the calcium hydroxide and magnesium hydroxide products was assessed according to Chinese industry standards HG/T 4120-2009 and HG/T 3607-2024, respectively. To optimize the process, a Box-Behnken design (BBD) within the response surface methodology (RSM) was employed using Design-Expert 13.0 software. This design was used to investigate the multivariate effects on the leaching rates of calcium and magnesium and to identify the optimal conditions. Furthermore, the leaching kinetics were calculated, the reaction activation energy was determined, and a corresponding kinetic model was established.

3. Results and discussion

3.1. Analysis of phosphate tailings

The chemical analysis results (Table 1) and mineralogical characteristics (Fig. 2) of the roasted phosphate tailings demonstrate that the phosphate tailings were mainly composed of dolomite, fluorapatite, and quartz, and that calcium, magnesium, phosphorus, and silicon were uniformly distributed in the spherical inclusions. In the roasted phosphate tailings, $CaMg(CO_3)_2$ in dolomite was completely decomposed into CaO and MgO, and $Ca_5F(PO_4)_3$ in apatite was retained.

Table 1. Mass fraction of each oxide in the phosphate tailings

Component	P_2O_5	CaO	MgO	SiO_2	Fe_2O_3	F	Al_2O_3
Wt/%	6.48	30.84	15.75	6.18	0.64	0.59	< 0.50

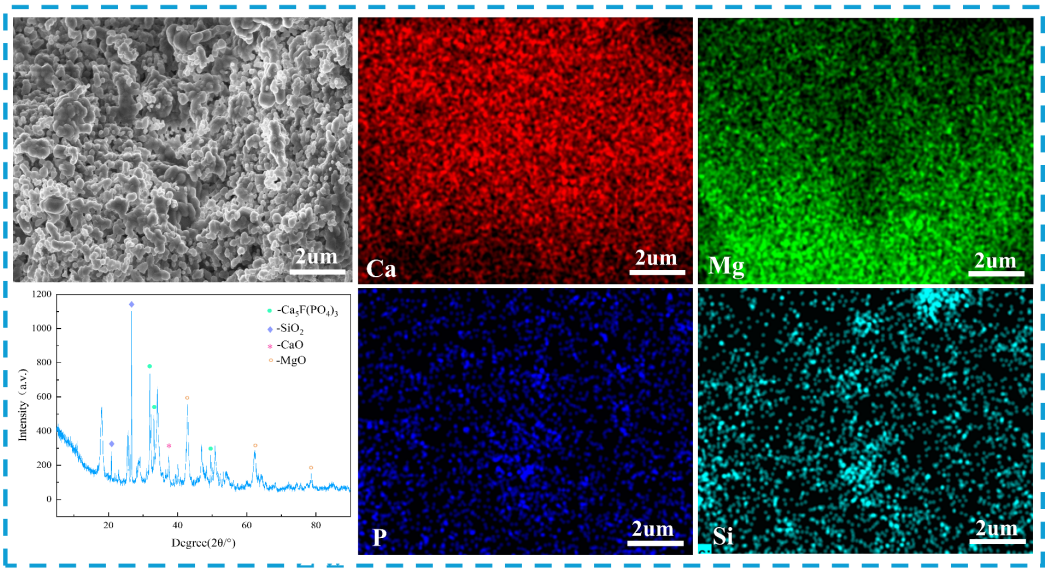

Fig. 2 Mineralogical characteristics of calcined phosphate tailings

3.2. Calcium-leaching test

3.2.1. Effect of single factors on the calcium-leaching rate

The effects of the type of ammonium salt (ammonium chloride, ammonium acetate, ammonium sulfate, and ammonium bicarbonate), dosage (mass ratio of roasted phosphate tailings and ammonium salts of 1:0, 1:0.4, 1:1, 1:1.5, 1:2, 1:2.5, or 1:3), reaction temperatures (20, 30, 40, 50, 60, and 80 °C), reaction times (10, 20, 40, 60, 80, 100, 120, and 150 min), liquid-to-solid ratio (1, 2.5, 5, 7.5, 10, 12.5, and 15), and pH (7.7, 8, 8.5, 9, 9.5, and 10) are shown in Fig.3. We first determined that ammonium chloride was the best salt for leaching. The optimum conditions were determined as follows: a mass ratio of roasted phosphate

tailings to ammonium chloride of 1:1, a temperature of 20 °C, a liquid-to-solid ratio of 10, a pH of 8.5, and a reaction time of 40 min. The leaching rates of calcium and magnesium under these optimum conditions were 85.36% and 0.5%, respectively.

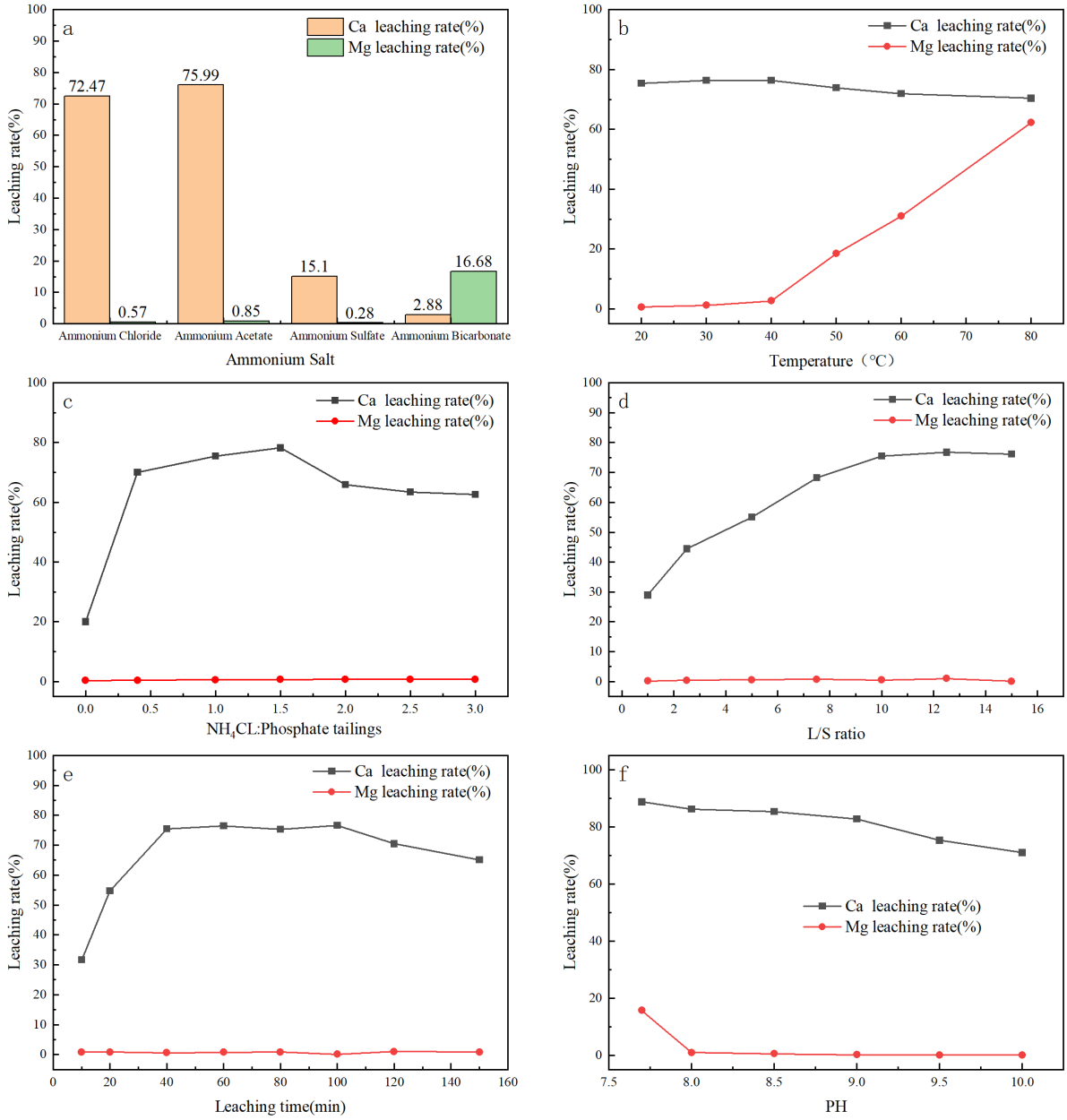

Fig. 3. Effect of single factors on the calcium-leaching rate

3.2.2. Surface-response optimization of calcium-leaching tests

To investigate the effects of the different factors on the calcium-leaching efficiency and optimize single-factor experimental conditions, we used a Box–Behnken design. Based on single-factor experiments showing no significant temperature effect, the reaction temperature was fixed at 20 °C. Three independent variables—ammonium chloride-to-roasted phosphate tailings mass ratio (A), liquid-to-solid ratio (B), and pH (C)—were selected, with calcium-leaching rate (Y) as the dependent variable (all factors and levels are listed in Table 2). Using Design-Expert 13.0, 17 experimental groups were designed via a three-factor, three-level Box–Behnken response-surface methodology to analyze A, B, and C. The results are shown in Table 3(Saadia et al., 2025; Yuan et al., 2022). A quadratic polynomial regression model was fitted to the data, as shown in Eq. (7):

$$Y = 83.75 + 3.80A + 9.63B - 5.71C - 1.03AB + 0.5875AC + 1.69BC - 6.24A^2 - 11.24B^2 - 4.35C^2 \quad (7)$$

The regression equation was analyzed with ANOVA, and the results are shown in Table 4. The F-value of the regression model was 296.37 with a P value of <0.0001, indicating that the model had high statistical significance. The P-value of the misfit term was 0.391, indicating that the difference between the two variables was not significant and that the model gave a good fit to the test results(Arroug et al., 2024; Khataee et al., 2011). The values of R^2 (0.9974) and R^2adj (0.9940) were close to 1, indicating a small model error and a high degree of accuracy in the regression equation, which can effectively represent the dependence of the rate of calcium leaching on the three independent variables(Wu et al., 2025). The effects of the primary terms A, B, and C ($P < 0.00010$), secondary terms A^2, B^2, and C^2 ($P < 0.00010$) were highly significant, whereas the effects of secondary terms AB and BC were significant ($P < 0.05$), and the effects of AC ($P > 0.05$) were not significant. The liquid-to-solid ratio had the greatest effect on the calcium-leaching rate, followed by pH and the amount of ammonium salt.

Based on the ANOVA of the regression model, the response surface and contour plots of each interaction term were visualized using Design-Expert 13.0 software to observe the effect of each factor on the calcium-leaching rate(Yang et al., 2017; Balasubramanian et al., 2009). For the interaction of A–B and B–C(Fig. 4(a) and Fig. 4(b)), the surface inclination of the 3D curve of the response surface was high, indicating strong interaction; by contrast, for the interaction of A–C (Fig. 4(c)), the surface inclination was not high, indicating minimal interaction of these two factors. From these response-surface plots, we made the following conclusions: (1) as the pH increased, the calcium-leaching rate decreased, indicating that lower pH levels promoted calcium leaching (A–B interaction); (2) with increasing drug-to-mineral ratio, the leaching rate first increased and then decreased, with a ratio of approximately 1 being ideal for calcium leaching (B–C interaction); and (3) with an increase of liquid-to-solid ratio, the leaching rate also first increased before decreasing, with an optimal ratio of approximately 1 (A–C interaction).

To achieve a balance between process economy and leaching efficiency, while reducing the amount of chemicals used and the liquid-to-solid ratio, DesignExpert 13.0 was used to optimize the objective function. The optimal leaching conditions determined at a temperature of 20 °C were: a mass ratio of ammonium chloride to roasted phosphate tailings of 0.98, a liquid-to-solid ratio of 9.78, and a pH of 8.5. Under these conditions, the calcium-leaching rate was 84.67%.

Table 2. Experimental design factors and levels for the response surface

Level	Factor		
	A	B	C
-1	0.5	5	8
0	1	10	9
1	1.5	15	10

Table 3. Test results for the response surface

Pilot program	A	B	C	Ca efficiency/%
1	0	0	0	83.58
2	-1	1	0	72.43
3	1	-1	0	62.16
4	0	0	0	83.81
5	-1	-1	0	52.11
6	1	1	1	74.45
7	1	0	-1	82.07
8	0	0	0	84.09
9	-1	0	1	63.06
10	1	1	0	78.37
11	0	-1	1	50.83
12	0	1	-1	82.10
13	-1	0	-1	76.05
14	0	0	0	84.74
15	0	0	0	82.52
16	0	-1	-1	62.25
17	1	0	1	71.43

Table 4. Analysis of variance

Source	Sum of Squares	df	Mean Square	F-value	P-value
Model	1983.60	9	220.40	296.37	＜0.0001
A	115.37	1	115.37	155.13	＜0.0001
B	741.13	1	741.13	996.57	＜0.0001
C	261.06	1	261.06	351.04	＜0.0001
AB	4.22	1	4.22	5.68	0.0487
AC	1.38	1	1.38	1.86	0.2152
BC	11.46	1	11.46	15.41	0.0057
A^2	164.09	1	164.09	220.65	＜0.0001
B^2	571.73	1	531.73	715.01	＜0.0001
C^2	79.77	1	79.77	107.27	＜0.0001
Residual	5.21	7	0.7437		
Lack of Fit	2.56	3	0.8549	1.29	0.3910
Pure Erro	2.64	4	0.6603		
Cor Total	1988.81	16			
R^2	0.9974				
R^2_{adj}	0.9940				
Adeq Precision	49.3200				

Note: $P < 0.01$, highly significant; $P < 0.05$, significant; $P > 0.05$, not significant

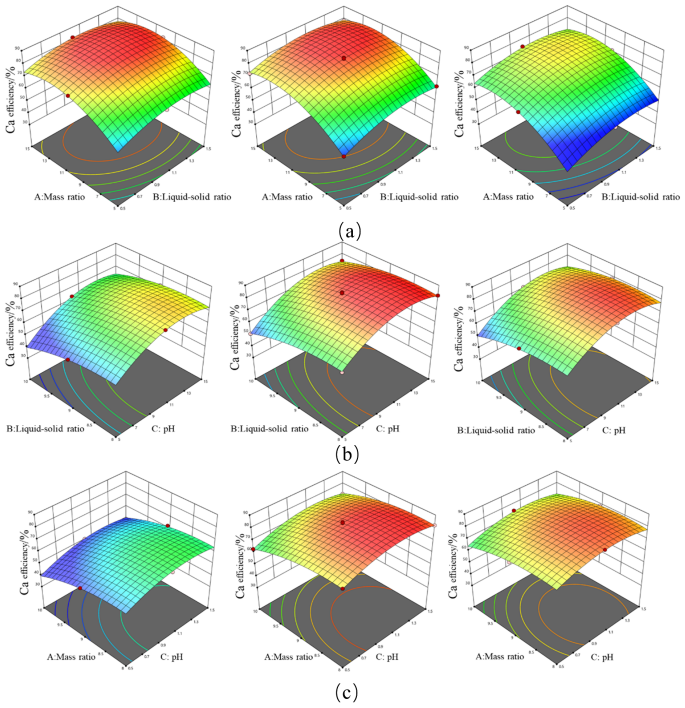

Fig. 4. Response-surface plots for two-way interactions: (a) A–B interactions, (b) B–C interactions, (c) A–C interactions

3.2.3 Kinetic analysis of calcium leaching

The dominant reaction mechanisms can be determined based on the relationship between the leaching rate and reaction conditions. The liquid-solid leaching process is controlled by the following mechanisms: external diffusion, internal diffusion, and surface chemistry (Li et al., 2025; Ma et al., 2025; Zhong et al., 2024; Lv et al., 2023; Ait Brahim et al., 2022; Wan et al., 2021; Madakkaruppan et al., 2016; An et al., 2014).

When the leaching reaction is controlled by external diffusion, the kinetic equation can be simplified as:

$$x = k_1 t \tag{8}$$

If the reaction is controlled by internal diffusion, it can be expressed as:

$$1 + 2(1 - x) - 3(1 - x)\text{^}(2/3) = k_2 t \tag{9}$$

If controlled by surface chemical reactions, the kinetic equation is expressed as:

$$1 - (1 - x)\text{^}(1/3) = k_3 t \tag{10}$$

According to Arrhenius' theorem, k = k0e−E/RT. Taking the logarithms on both sides of this equation yields the integral equation:

$$lnk = lnk_0 - \frac{E}{RT} \tag{11}$$

where x is the reacted fraction, t is the reaction time (min), k is the reaction rate constant, T is the reaction temperature (K), R is the molar gas constant (8.3145 J/mol), and E is the reaction activation energy (J/mol).

In the one-way test, the calcium-leaching rate from phosphate tailings was not linearly related to time. Therefore, the equations of the external-diffusion-control model were poorly correlated. The experimental leaching rates obtained at different temperatures were used in Eqs (9) and (10), the calculations from which were linearly fitted with the leaching time to obtain the corresponding value of k. The activation energy of the leaching process and the correlation coefficient, R^2, were calculated to determine the reaction-control model based on the Arrhenius equation.

The leaching experiments were conducted under the following conditions: a ratio of ammonium chloride to roasted phosphate tailings of 0.98:1, a liquid-to-solid ratio of 9.78:1, a pH of 8.5, and a stirring rate of 500 r/min. The leaching time was varied (10, 20, 30, and 40 min) under different temperatures (293.15, 303.15, 313.15, and 323.15 K). The obtained calcium-leaching rates were used in Eq. (9) and Eq. (10) to obtain the linear fitting results shown in Fig. 5; the slope of the straight line obtained from the fitting is k. The linear fitting parameters are shown in Table 5. The apparent activation energy of the model and R^2 were obtained from Eq. (11) by using the data in Table 6. The R^2 of the internal diffusion model was 0.96396, and the activation energy of the reaction was less than 20 kJ. Thus, it can be concluded that the calcium leaching process in phosphate tailings is best described as internal diffusion, which can be characterized by the following kinetic equation (12):

$$1 + 2(1 - x) - 3(1 - x)\text{^}(2/3) = 3.7234 \times 10\text{^}(-2) exp(-2.2436 \times 10\text{^}(3)/RT)t \tag{12}$$

However, its exceptionally low apparent activation energy (2.24 kJ/mol) falls far below the typical range for internal diffusion (10–20 kJ/mol), indicating that this diffusion process is not diffusion in the conventional sense. This may be attributed to the calcination pretreatment forming a highly permeable structure with numerous interconnected pores, rather than a dense product diffusion barrier layer. These pores provide low-resistance pathways for both the leaching agent and the products, significantly reducing the energy barrier for ion transport. This results in the extremely low activation energy observed.

Table 5. Fitting results of the internal-diffusion and chemical-reaction models

reaction temperature /K	Internal diffusion control model		Chemical reaction control modeling	
	K_2	R_2^2	K_3	R_3^2
293.15	0.00114	0.98618	0.01221	0.97633
303.15	0.01179	0.98641	0.01243	0.97408
313.15	0.01237	0.99807	0.01294	0.97562
323.15	0.01268	0.99058	0.01325	0.9737

Table 6. Fitting results for the Arrhenius model

control model	reaction activation energy E/	R^2
Internal diffusion control model	2.24	0.96396
Chemical reaction control modeling	2.47	0.90537

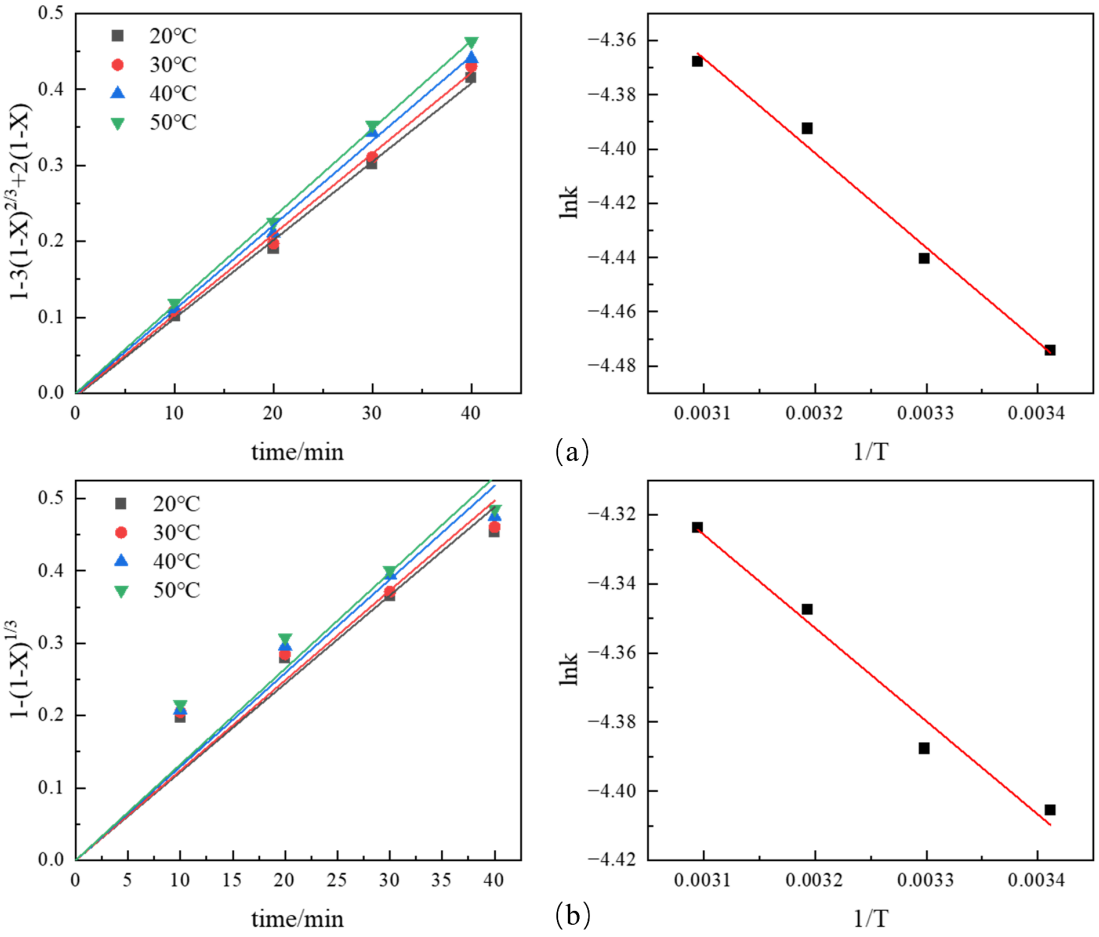

Fig. 5(a). Fitting curve and activation energy for the internal-diffusion-control model of calcium leaching, (b) Fitting curve and activation energy for the chemical-reaction-control model of calcium leaching

3.3. Magnesium-leaching test

3.3.1. Effect of single factors on the magnesium-leaching rate in primary leaching slag

MgO exhibits limited hydration at ambient temperature, predominantly retaining its oxide form. Thermally activated ammonium sulfate selectively converts MgO to soluble $MgSO_4$ while precipitating residual $Ca(OH)_2$ as $CaSO_4$, effectively suppressing calcium dissolution in leachates and validating its efficacy for magnesium extraction. We analyzed the effect of ammonium sulfate dosage (with mass ratios of ammonium sulfate to primary leaching residue of 1:0, 1:0.5, 1:1.3, 1:2, 1:2.6, 1:3.3, and 1:4), reaction temperature (20, 30, 40, 50, 60, 70, 80, and 90 °C), reaction time (20, 40, 60, 80, 100, 120, and 150 min), liquid-to-solid ratio (1.3, 3.3, 6.7, 10, 13.3, 16.7, and 20) and other experimental conditions. The results are shown in Fig. 6. We determined the optimized conditions to be as follows: primary leaching residue to ammonium sulfate mass ratio of 1:1.3, temperature of 80 °C, liquid-to-solid ratio of 13.3, and a reaction time of 60 min. Under these conditions, the magnesium- and calcium-leaching rates reached 95.42% and 1.81%, respectively.

3.3.2 Surface-response optimization of magnesium-leaching tests

Single-factor experiments revealed that a pH of 7 significantly enhanced magnesium leaching efficiency while offering favorable acid-base stability with minimal environmental impact, leading to its exclusion from further optimization processes. The experimental design was optimized using three independent variables—ammonium sulfate-to-primary leaching residue mass ratio (A), liquid-to-solid ratio (B), and temperature (C), with the magnesium-leaching rate (Y) as the dependent variable (all factors and levels are shown in Table 7). Using Design-Expert 13.0, 17 experiments were designed via a Box–Behnken

response-surface methodology for a three-factor, three-level analysis of A, B, and C. The results are shown in Table 8. The following quadratic polynomial regression model was fitted to the data, as shown in Eq. (13):

$$Y = 61.99 + 3.4A + 5.47B + 9.47C - 0.2675AB + 0.0450AC - 1.10BC - 5.82A^2 - 5.81B^2 - 9.49C^2 \quad (13)$$

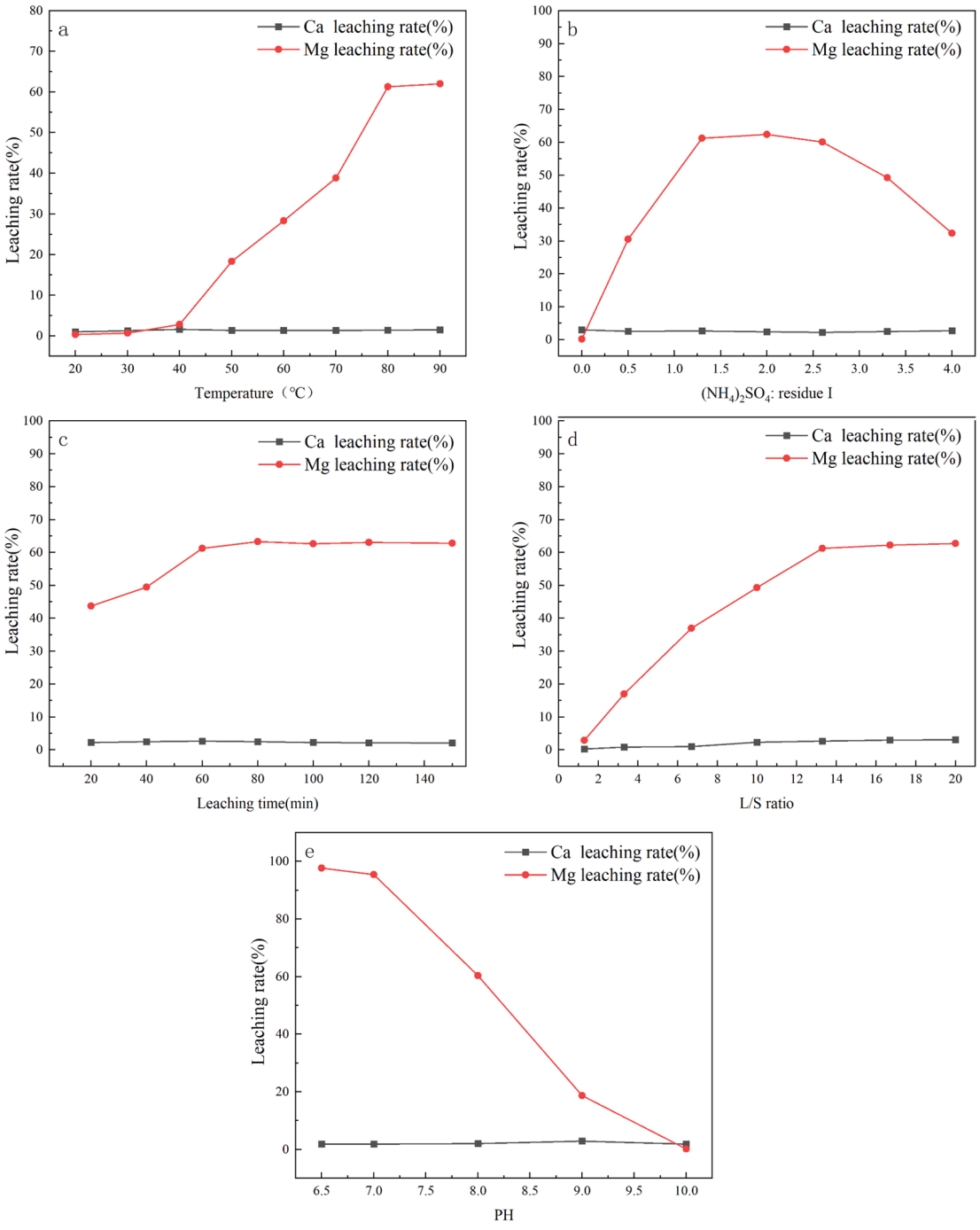

Fig. 6. Effect of single factors on the magnesium-leaching rate

Table 7. Experimental design factors and levels for the response surface

Level	Factor		
	A	B	C/℃
-1	0.8	8.3	70
0	1.3	13.3	80
1	1.8	18.3	90

Table 8. Test results for the response surface

Pilot program	A	B	C	Mg efficiency/%
1	1	-1	0	48.39
2	0	1	1	60.08
3	0	0	0	62
4	0	0	0	61.26
5	0	1	-1	43.33
6	-1	0	1	53
7	0	-1	-1	31.09
8	-1	1	0	52.86
9	0	-1	1	52.25
10	1	1	0	59.71
11	-1	-1	0	40.47
12	-1	0	-1	34.05
13	0	0	0	61.89
14	0	0	0	62.75
15	0	0	0	62.04
16	1	0	1	59.3
17	1	0	-1	40.27

The regression equation was analyzed with ANOVA, and the results are shown in Table 9. The F-value of the regression model was 401.43, with a P-value of < 0.0001, indicating that the regression model was highly statistically significant. The P-value of the misfit term was 0.1738, meaning that the difference between the two variables was not significant. Thus, the model fitted the test results well. The R^2 and R^2adj of the model (0.9981 and 0.9956, respectively) were close to 1. This indicates a small model error and a high degree of accuracy in the regression equation, which can effectively represent the dependence of the magnesium-leaching rate on the mass ratio of ammonium salts to roasted phosphate tailings, the liquid-to-solid ratio, and temperature(Wu et al., 2025). The primary terms A, B, and C ($P < 0.00010$), the secondary terms A^2, B^2, and C^2 ($P < 0.00010$) had highly significant effects, the secondary term BC had a significant effect ($P < 0.05$), and AB and AC ($P > 0.05$) had insignificant effects. In addition, the factor with the greatest effect on the magnesium-leaching rate was the temperature, followed by the liquid-to-solid ratio and the amount of ammonium salt used.

Table 9 Analysis of variance

Source	Sum of Squares	df	Mean Square	F-value	P-value
Model	1790.82	9	198.98	401.43	＜0.0001
A	92.41	1	92.41	186.44	＜0.0001
B	239.59	1	239.59	483.36	＜0.0001
C	718.02	1	718.02	1448.57	＜0.0001
AB	0.2862	1	0.2862	0.5774	0.4721
AC	0.0081	1	0.0081	0.0163	0.9019
BC	4.86	1	4.86	9.81	0.0166
A^2	142.57	1	142.57	287.63	＜0.0001
B^2	142.20	1	142.20	286.89	＜0.0001
C^2	379.12	1	379.12	764.86	＜0.0001
Residual	3.47	7	0.4957		
Lack of Fit	2.35	3	0.7822		
Pure Erro	1.12	4	0.2808		
Cor Total	1794.29	16			
R^2	0.9981				
R^2_{adj}	0.9956				
Adeq Precision	58.0570				

Note: $P < 0.01$, highly significant; $P < 0.05$, significant; $P > 0.05$, not significant

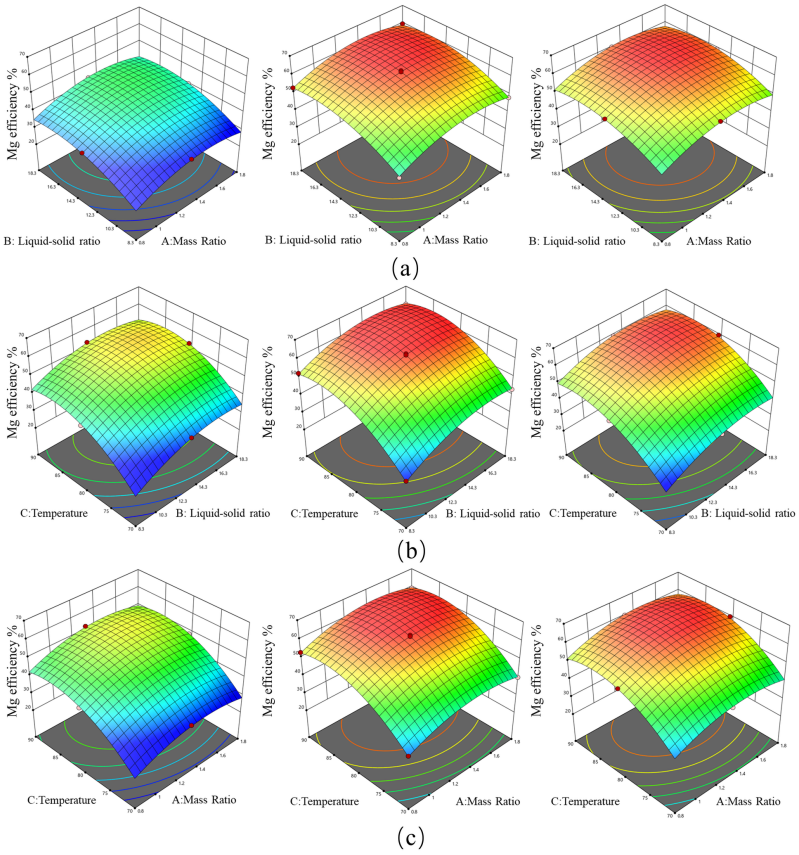

Fig. 7. Response-surface plots for two-way interactions: (a) A–B interactions, (b) B–C interactions, (c) A–C interactions

Based on the ANOVA of the regression model, the response surface and contour plots of each interaction term were plotted using Design-Expert 13.0 software to visualize their effects on the leaching rate of magnesium (Fig. 7). For the interaction of A–C and B–C, the inclination of the 3D curve of the response surface was higher, indicating a strong interaction of these factors; for the interaction of A–B, the inclination was not high, indicating that the interaction of these factors was weak. From the A–B interaction, we conclude that an increase in temperature had a strong promoting effect on leaching. From the B–C interaction, the leaching rate initially increased and then decreased with an increase in the drug-to-mineral ratio, with an optimal ratio of around 1.3. From the A–C interaction, the leaching rate first increased and then decreased with increasing liquid-to-solid ratio, with an optimum ratio of about 13.3.

To achieve a balance between process economy and leaching efficiency, the objective function was optimized using Design-Expert 13.0. Under the optimal leaching conditions (85.14 °C, a mass ratio of ammonium sulfate to primary leaching residue of 1.2, a liquid-to-solid ratio of 12.1, and a pH of 7), a magnesium-leaching rate of 95.21% was achieved.

3.3.3. Kinetic analysis of magnesium leaching

The one-way test results showed that the reaction time did not have a linear effect on the magnesium-leaching rate. This suggests a poor correlation with the equation of the external-diffusion-controlled model. We conducted experiments using the primary leaching slag as the raw material, a mass ratio of ammonium sulfate to the raw material of 1.2:1, a liquid-to-solid ratio of 12.1:1, a pH of 7, and a stirring rate of 500 r/min. We varied the leaching time (20, 40, 60, and 80 min) and temperature (313.15, 323.15, 333.15, 343.15, and 353.15 K). The resulting magnesium-leaching rate data were used in Eqs (9) and (10) to obtain the linear fitting results in Fig. 8; the slope of the straight line obtained from the fitting was k. The linear fitting parameters are shown in Table 10. The apparent activation energy of the model and R^2 were obtained from Eq. (11) using the data in Table 11. The R^2 of the chemical-reaction model

(0.94765) was larger than that of the internal-diffusion model (0.93026). With an activation energy in the range of 20–40 kJ, the magnesium-leaching reaction was chemical-reaction-controlled. The reaction rate of the chemical reaction was a function of the temperature, with a higher activation energy corresponding to a stronger dependence. The results obtained correspond to the effect of temperature on magnesium leaching in the one-factor condition test. Thus, the kinetic equation for magnesium leaching was shown in Eq. (14):

$$1-(1-x)\text{^}(1/3)=3.4099\times 10\text{^}(3)exp(-3.7564\times 10\text{^}(4)/RT)t \quad (14)$$

Table 10. Fitting results for the internal-diffusion and chemical-reaction models

reaction	Internal diffusion control model		Chemical reaction control modeling	
temperature /K	K_2	R_2^2	K_3	R_3^2
313.15	0.000469485	0.94201	0.00161	0.99822
323.15	0.00199	0.95847	0.00347	0.9931
333.15	0.00313	0.9878	0.00454	0.98244
343.15	0.0047	0.99477	0.00578	0.97577
353.15	0.01006	0.99117	0.00956	0.96572

Table 11. Fitting results for the Arrhenius model

Control model	Reaction activation energy E/ (kJ/mol)	R^2
Internal diffusion control model	64.62	0.93026
Chemical reaction control modeling	37.58	0.94765

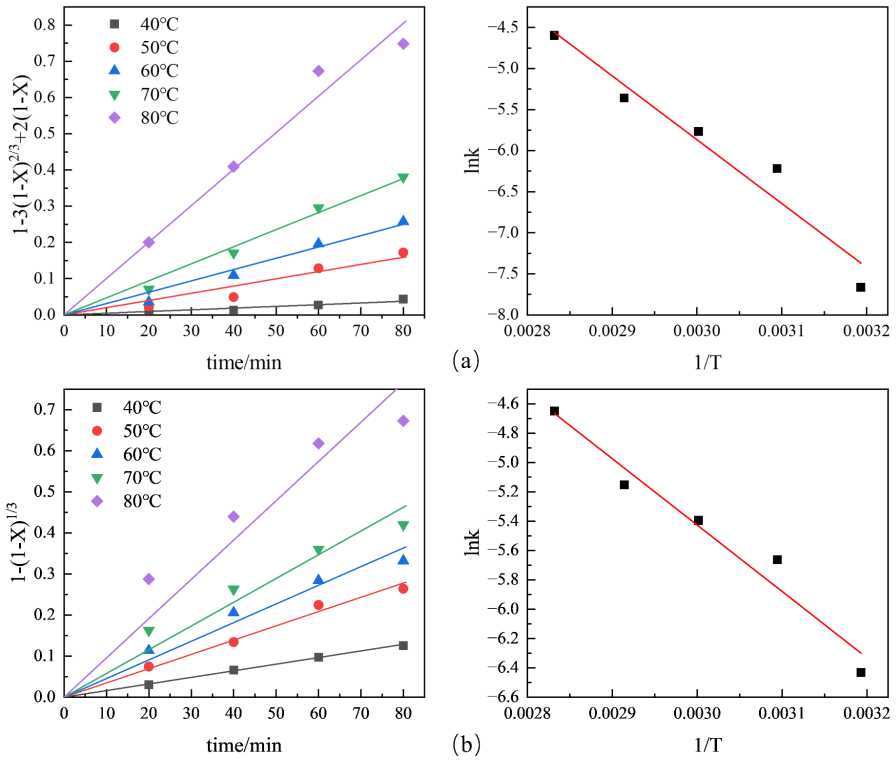

Fig. 8(a) Fitting curve and activation energy for the internal-diffusion-control model of magnesium leaching, (b) Fitting curve and activation energy for the chemical-reaction-control model of magnesium leaching

3.4. Topographic analysis

The morphological evolution of phosphate tailings during roasting and leaching was revealed by laser particle sizing and SEM-EDS analysis. These results, in addition to the particle size distribution of the three samples (Fig. 9) and SEM mapping (Fig. 10(a)), revealed that the surfaces of the original samples were irregularly flaky, angular, or lumpy, with uneven texture. The particle size was initially

concentrated in the diameter range of 0–70 μm. During roasting, the high temperature melted minerals or softened their surface. This resulted in the agglomeration of particles with high sphericity and round boundaries and a loss of their original angular structure. The size range increased to 0–90 μm. After leaching, the smooth spherical agglomerates formed by roasting disintegrated owing to the selective leaching of calcium and magnesium from dolomite ($CaMg(CO_3)_2$). This process disrupted the interface between apatite ($Ca_5(PO_4)_3F$) and dolomite and caused the crystals to lose their encapsulating effect, re-exposing their intrinsic morphology and forming distinct phase regions. The overall structure changed from a dense spherical form to a loose, porous network, and the grain size was concentrated in the range of 0–50 μm. The primary apatite crystals have a typical hexagonal columnar crystal structure, with prismatic and detrital surfaces visible on their surface(Hamza et al., 2024; Michie et al., 2008).

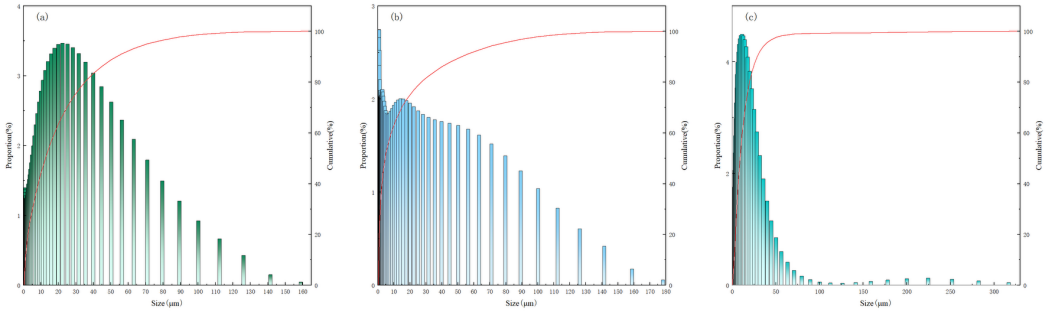

Fig. 9. Laser particle-size analysis: (a) raw ore, (b) roasted phosphate tailings, and (c) residue

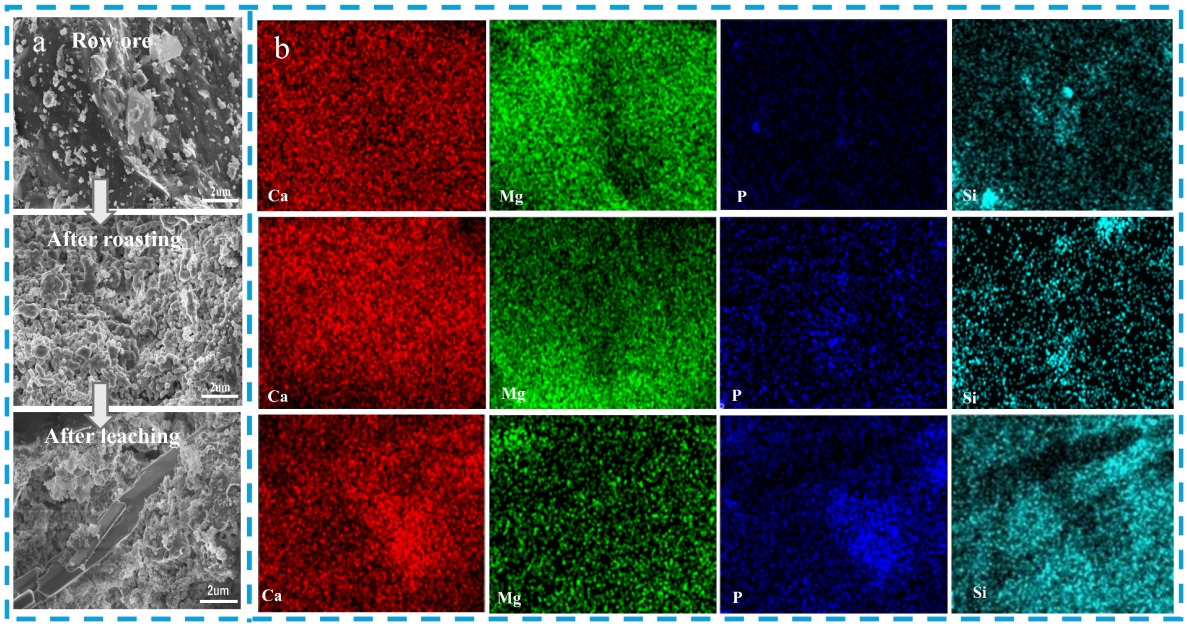

Fig. 10. SEM-EDS comparative analysis of phosphogypsum and its calcined and leached samples. (a) SEM image of the sample; (b) corresponding elemental distribution maps for Ca, Mg, P, and Si

The surface energy spectra (EDS) of the three samples are shown in Fig. 10(b). The signals of calcium and magnesium were weakened after selective leaching, whereas those of phosphorus and silicon were enhanced. The enriched areas of calcium and phosphorus signals were highly coincident with the spatial locations of the residual columnar apatite crystals. These findings demonstrate that the selective leaching process preferentially removes calcium and magnesium from dolomite, exposing the intrinsic structure of apatite crystals and providing a basis for calcium and magnesium separation and the subsequent efficient recovery of phosphorus.

3.5. Comprehensive utilization of Ca and Mg in leachate

A two-step precipitation process was adopted. NaOH was introduced into each leachate to adjust the pH, selectively precipitating calcium and magnesium as their respective hydroxides. Following solid-liquid separation and drying, the resulting products were identified as high-purity calcium hydroxide (Product I) and magnesium hydroxide (Product II), with minimal impurities, consistent with the XRD patterns shown in Fig. 11.

In Leachate I, the pH was adjusted to 12 using NaOH, which provided sufficient OH^- to precipitate calcium ions almost completely as calcium hydroxide. Product I assayed >98% $Ca(OH)_2$ (Table 12 for complete characterization data) and conformed to the HG/T 4120-2024 standard for Industrial Calcium Hydroxide (Type 95). This high-purity product is suitable for manufacturing bleaching agents, calcium-based compounds, and thermal stabilizers, and finds applications in water treatment, soil remediation, dye dispersion, flue gas desulfurization, coatings, and building materials. In Leachate II, the pH was raised to 12.5, enabling Mg^{2+} to react with OH^- and precipitate as magnesium hydroxide, achieving nearly complete magnesium recovery. Product II assayed >88% $Mg(OH)_2$ (3.6. Economic **analysis**
This study developed a resource utilization process for phosphate tailings based on two-step ammonium salt leaching and ammonia gas recycling. Economic analysis indicates that processing one ton of tailings yields approximately 245.96 kg of calcium hydroxide and 218.12 kg of magnesium hydroxide, with the main products generating a value of 812 yuan. Additionally, the phosphorus-rich leaching residue (P_2O_5 > 17%) serves as high-quality flotation feedstock, creating an additional value of 70 yuan, resulting in a comprehensive output value of 882 yuan.

Table 13 for complete characterization data) and satisfied the requirements for Type II-B Magnesium Hydroxide as per the HG/T 3607-2024 standard. Its typical applications include use as a flame retardant precursor, wastewater treatment agent, agricultural fertilizer additive, and soil ameliorant.

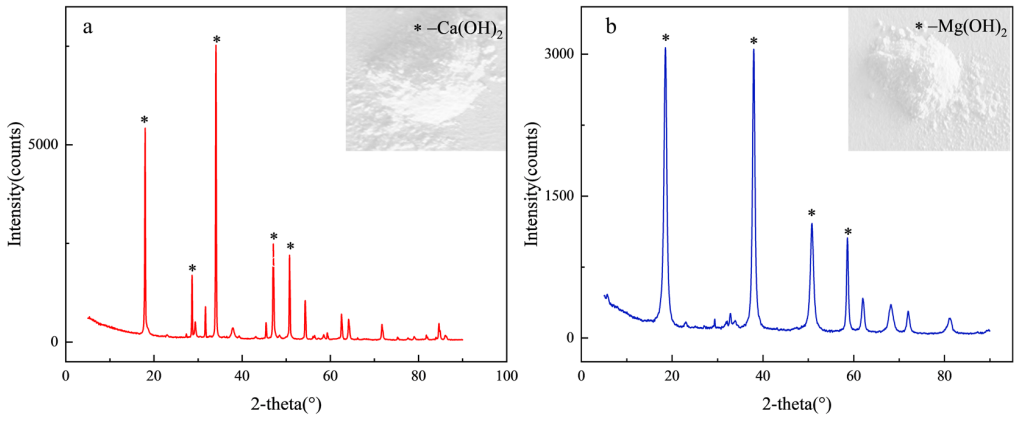

Fig. 11. XRD pattern of the precipitated product: (a) Product I, (b) Product II

Table 12. Comparison of Product I with HG/T 4120-2024 Industry Standard

Item		Indicator				Product I
		96	95	90	85	96
Calcium Hydroxide [$Ca(OH)_2$] w/%≥		96.0	95.0	90.0	85.0	98.16
Free calcium oxidew/%≤		0.5	2.5	—	—	0.46
Magnesium Oxide w/%≤		1.0	1.5	—	—	0.64
Matter Insoluble in Hydrochloric Acid w/%≤		0.10	0.25	1.0	—	0.08
Iron (Fe) w/%≤		0.05	0.10	—	—	0.0044
Loss on drying w/%≤		0.5	1.0	1.0	1.0	0.45
Fineness	(Residue on 0.045 mm Test Sieve) w/%≤	5.0	5.0	—	—	4.86
	(Residue on 0.075 mm Test Sieve) w/%≤	—	—	5.0	12.0	2.65
Heavy Metals (as Pb) w/%≤		0.002	—	—	—	0.5×10^{-6}

3.6. Economic analysis

This study developed a resource utilization process for phosphate tailings based on two-step ammonium salt leaching and ammonia gas recycling. Economic analysis indicates that processing one ton of tailings yields approximately 245.96 kg of calcium hydroxide and 218.12 kg of magnesium hydroxide, with the main products generating a value of 812 yuan. Additionally, the phosphorus-rich leaching residue (P_2O_5 > 17%) serves as high-quality flotation feedstock, creating an additional value of 70 yuan, resulting in a comprehensive output value of 882 yuan.

Table 13. Comparison of Product II with HG/T 3607-2024 Industry Standard

Item		Indicator					Produ Ⅱ
		Ⅰ			Ⅱ		Ⅱ
		Ⅰ-A	Ⅰ-B	Ⅰ-C	Ⅱ-A	Ⅱ-B	Ⅱ-B
Magnesium Hydroxide (on dry basis) w/%≥		99.5	99.0	98.5	90.0	85.0	88.43
Calcium Oxide (CaO) w/%≤		0.05	0.05	0.5	2.0	3.0	2.40
Matter Insoluble in Hydrochloric Acid w/%≤		0.1	0.1	0.1	5.0	10.0	0.18
Moisture w/%≤		0.5	0.5	0.5	0.5	0.5	0.47
Chloride (as Cl) w/%≤		0.1	0.6	0.1	0.05	0.05	0.025
Iron (Fe) w/%≤		0.005	0.005	0.05	0.35	0.35	0.0041
Loss on ignition w/%≥		30.0	30.0	30.0	28.0	26.0	26.24
Whiteness (Wr)≥		98	95	92	90	88	91.6
Residue on 45 μm Test Sieve w/%≤		0.05	—	0.05	0.05	0.05	0.03
Laser particle size	D_{50}/um≤	2	—	5	—	—	16.4
	D_{90}/um≤	5	—	10	—	—	35
Specific surface area (on dry basis)/(m^2/g)≤		10	—	—	—	—	—

Compared to traditional sulfuric or hydrochloric acid leaching processes, this technology employs an ammonia gas recycling system, significantly reducing chemical consumption costs. Furthermore, the near-neutral leaching system effectively mitigates corrosion of reaction equipment caused by strong acid environments, projected to decrease equipment maintenance frequency by approximately 40% and substantially reduce maintenance expenditures. Significant additional economic benefits are generated through chemical savings, reduced equipment maintenance costs, elimination of tailings storage expenses, and decreased environmental remediation costs. The resource recycling model established by this research provides a solution for phosphorus tailings management in environmentally sensitive areas like the Dianchi Lake basin, achieving synergistic enhancement of both economic and ecological benefits.

4. Conclusions

This study proposes a two-stage ammonium salt leaching process integrated with an ammonia recovery system, achieving efficient separation of calcium, magnesium, and phosphorus from calcined phosphate tailings. This process yields economically valuable calcium and magnesium products while achieving zero residue discharge.

(1) The near-neutral pH in both leaching stages complies with the principles of green chemistry, giving it a significant advantage over traditional acid leaching methods. The mechanism of ammonia recycling minimizes exhaust emissions while also substantially reducing reagent consumption and operating costs, thereby providing a sustainable solution for increasing the resource utilization of phosphate tailings.

(2) The maximum calcium- and magnesium-leaching rates from the phosphate tailings were 84.67% and 95.21%, respectively, and the phosphorus grade of the tailings was 17. Achieving efficient separation and recovery of calcium, magnesium, and phosphorus while producing Type 96 calcium hydroxide compliant with HG/T 4120-2024 and Type II-B magnesium hydroxide compliant with HG/T 3607-2024, delivering significant economic and environmental benefits.

(3) Using the unreacted shrinking core model' and Arrhenius' law, we determined that calcium leaching was controlled by internal diffusion, with an activation energy of 2.24 kJ/mol. The kinetic equation

for calcium leaching was derived as: $2(1-x)-3(1-x)^{2/3}=3.7234\times10^{-2}\cdot\exp(-2.2436\times10^{-2}/RT)t$. By contrast, for magnesium leaching, the reaction was governed by chemical reactions, with an activation energy of 37.58 kJ/mol. The corresponding kinetic equation was established as: $1-(1-x)^{1/3}=3.4099\times10^{3}\exp(-3.7584\times10^{4}/RT)t$.

Acknowledgment

This work was supported by the Open Fund of the National Engineering Research Center for the Development and Utilization of Phosphate Resources (No. NECP2023-10). The authors are grateful to Prof. Tong (Kunming University of Science and Technology) for his valuable suggestions and insightful discussions. We also sincerely appreciate the assistance provided by the members of his research group during the experimental and analytical phases of this work.

Reference

AIT BRAHIM, J., AIT HAK, S., ACHIOU, B., BOULIF, R., BENIAZZA, R., BENHIDA, R., 2022. *Kinetics and mechanisms of leaching of rare earth elements from secondary resources.* Miner. Eng. 177, 107351.

AMAR, H., BENZAAZOUA, M., ELGHALI, A., HAKKOU, R., TAHA, Y., 2022. *Waste rock reprocessing to enhance the sustainability of phosphate reserves: A critical review.* Journal of Cleaner Production 381, 135151.

AN, J., YANG, W., YIN, J., YUAN, X., ZHOU, X., XIA, W., 2014. *Kinetics of phosphorus removal from high-phosphorus iron ores by HCl leaching.* Explor. Process. Miner. Resour. 455–458.

ARROUG, L., ELAATMANI, M., ZEGZOUTI, A., 2024. *A preliminary study to investigate the beneficiation of low-grade phosphate sludge using reverse flotation: Modeling and optimization through Box-Behnken design and response surface methodology.* Chem. Eng. Res. Des. 204, 228–237.

BALASUBRAMANIAN, V., LAKSHMINARAYANAN, A., VARAHAMOORTHY, R., BABU, S., 2009. *Application of Response Surface Methodolody to Prediction of Dilution in Plasma Transferred Arc Hardfacing of Stainless Steel on Carbon Steel.* J. Iron Steel Res. Int. 16, 44–53.

CHEN, B., JIN, C., YANG, J., QU, G., LIU, Y., WU, F., LIU, S., LIU, X., 2024. *Synergistic organic manure treatment with Al/Fe/Ca-based fluoride-fixing agents promote soil formation and utilization of phosphate flotation tailings.* Process Saf. Environ. Prot. 192, 495–509.

DING, S., YIN, L., ZHANG, T., LV, L., TANG, W., TANG, S., 2025. *Resource utilization of phosphate tailings by calcination and leaching with dilute H_3PO_4 solution.* Miner. Eng. 222.

FU, F., HU, N., YE, Y., CHEN, G., GUAN, W., YANG, S., LI, Q., 2024. *Production of high-value-added lightweight glass ceramics based on phosphorus tailings and coal gangue.* Ceram. Int. 50, 16725–16735.

GU, H., ZHOU, G., WEN, H., WANG, N., 2025. *Using of phosphoric acid to dissolve phosphate ore flotation tailings for stepwise separation of calcium and magnesium values.* Chem. Eng. Sci. 307, 121356.

HAMZA, M., HAMDI, B., BEN AHMED, A., CAPITELLI, F., EL FEKI, H., 2024. *Synthesis of a new potassium-substituted lead fluorapatite and its structural characterization.* RSC Adv. 14, 16876–16885.

JIANG, W., JIANG, Y., LI, P., LIU, D., REN, Y., LI, D., LIU, Z., CHEN, Y., YE, Y., 2023. *Reuse of phosphogypsum and phosphorus ore flotation tailings as adsorbent: The adsorption performance and mechanism of phosphate.* J. Phys. Chem. Solids. 178.

KHATAEE, A.R., KASIRI, M.B., ALIDOKHT, L., 2011. *Application of response surface methodology in the optimization of photocatalytic removal of environmental pollutants using nanocatalysts.* Environ. Technol. 32, 1669–1684.

LI, T., LI, G., LIU, X., SUN, J., LU, Q., CUI, Z., 2025. *Enhanced oxidative sulfuric acid leaching of granite-type uranium ore by oxygen nanobubbles: Kinetics and mechanism.* Nucl. Eng. Technol. 57, 103608.

LV, N., CHEN, H., SU, C., WANG, H., DONG, Y., WU, L., 2023. *Kinetics Investigation of Phosphorus Leaching from Steelmaking Slag.* Miner. Process. Extr. Metall. Rev. 44, 571–576.

MA, Y., HU, C., JIN, Y., ZHEN, H., WU, J., YANG, L., 2025. *Recovery of ruthenium resources from red mud via phosphoric acid leaching: A comprehensive investigation of leaching effects and kinetics.* J. Clean. Prod. 486, 144423.

MA, Z., LI, D., YUE, S., YIN, X., WANG, C., ZHOU, C., MA, K., SONG, L., YUE, H., 2025. *Separation of calcium and magnesium from phosphorus tailings by the integrated CO_2 absorption-mineralization process.* Sep. Purif. Technol. 364.

MADAKKARUPPAN, V., PIUS, A., SREENIVAS, T., GIRI, N., SARBAJNA, C., 2016. *Influence of microwaves on the leaching kinetics of uraninite from a low grade ore in dilute sulfuric acid.* J. Hazard. Mater. 313, 9–17.

MICHIE, E.M., GRIMES, R.W., FONG, S.K., METCALFE, B.L., 2008. *Predicted energies and structures associated with the mixed calcium strontium fluorapatites.* J. Solid State Chem. 181, 3287–3293.

Mineral commodity summaries 2025 (Report No. 2025), 2025. , *Mineral Commodity Summaries. Reston*, VA.

SAADIA, S., HOUCINE, B., ABDELHAK, B., AHMED, M., 2025. *Optimization of factors affecting biogas production from dairy wastewater using Response Surface Methodology and its kinetic and microbial analysis.* Results Eng. 26, 104781.

WAN, J., DU, H., GAO, F., WANG, S., GAO, M., LIU, B., ZHANG, Y., 2021. *Direct Leaching of Vanadium from Vanadium-bearing Steel Slag Using NaOH Solutions: A Case Study.* Miner. Process. Extr. Metall. Rev. 42, 257–267.

WU, Z., LI, Y., ZHOU, W., FU, Q., 2025. *Multi-objective optimization of heat pump drying process using NSGA-II and response surface methodology: a case study of sludge*. Case Stud. Therm. Eng. 72, 106257.

XIAO, T., FAN, X., ZHOU, C., WANG, H., WU, K., ZHOU, H., 2024. *Preparation of ultra-lightweight ceramsite from waste materials: Using phosphate tailings as pore-forming agent.* Ceram. Int. 50, 15218–15229.

XIAO, Y., YAN, T., YAO, P., XIANG, W., WU, Y., LI, J., 2024. *Co-pyrolysis of sewage sludge and phosphate tailings: Synergistically enhancing heavy metal immobilization and phosphorus availability.* Waste Manag. 181, 44–56.

YANG, Y., WEI, Z., CHEN, Y., LI, Y., LI, X., 2017. *Utilizing phosphate mine tailings to produce ceramisite.* Constr. Build. Mater. 155, 1081–1090.

YE, J., CHEN, J., LUO, K., YAN, F., ZHANG, W., REN, X., LI, J., RONG, H., 2024. *The leaching model and leaching kinetics of lithium slag in alkaline solution.* Constr. Build. Mater. 432.

YU, Y., DU, C., YANG, X., 2023. *Recovery of phosphorus from steelmaking slag and phosphate tailings by a collaborative processing method.* Sep. Purif. Technol. 313.

YU, Y., DU, C., ZHANG, Y., YUAN, R., 2024. *Phosphorus recovery from phosphate tailings through a two-stage leaching-precipitation process: Toward the harmless and reduction treatment of P-bearing wastes.* Environ. Res. 248, 118328.

YUAN, X., LUO, F., CHEN, X., XIA, W., ZOU, Y., ZHOU, X., LIU, H., SONG, Y., HE, J., MA, S., 2022. *Effective Cu(II) ions adsorption from aqueous solutions using low grade oolitic hematite tailing with phosphorus: response surface methodology.* Desalin. Water Treat. 265, 57–70.

ZHONG, S., HU, M., ZHANG, L., LI, H., ZHANG, Q., RU, X., WANG, LI, A., 2024. *Leaching behavior and kinetics of beryllium in beryllium-containing sludge (BCS).* Environ. Pollut. 358, 124497.